

University of New Hampshire
University of New Hampshire Scholars' Repository

Center for Coastal and Ocean Mapping

Center for Coastal and Ocean Mapping

3-2015

Split-beam echosounder observations of natural methane seep variability in the northern Gulf of Mexico

Kevin W. Jerram

University of New Hampshire, Durham, kevin.jerram@unh.edu


Thomas C. Weber

University of New Hampshire, Durham, thomas.weber@unh.edu

Jonathan Beaudoin

University of New Hampshire, Durham

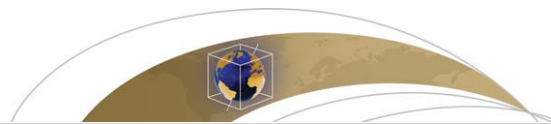
Follow this and additional works at: <https://scholars.unh.edu/ccom>

 Part of the [Geochemistry Commons](#), and the [Geophysics and Seismology Commons](#)

Recommended Citation

Jerram, K., T. C. Weber, and J. Beaudoin (2015), Split-beam echo sounder observations of natural methane seep variability in the northern Gulf of Mexico, *Geochem. Geophys. Geosyst.*, 16, 736–750, doi:10.1002/2014GC005429.

This Journal Article is brought to you for free and open access by the Center for Coastal and Ocean Mapping at University of New Hampshire Scholars' Repository. It has been accepted for inclusion in Center for Coastal and Ocean Mapping by an authorized administrator of University of New Hampshire Scholars' Repository. For more information, please contact nicole.hentz@unh.edu.



RESEARCH ARTICLE

10.1002/2014GC005429

Split-beam echo sounder observations of natural methane seep variability in the northern Gulf of Mexico

Kevin Jerram¹, Thomas C. Weber¹, and Jonathan Beaudoin¹¹Center for Coastal and Ocean Mapping, University of New Hampshire, Durham, New Hampshire, USA

Key Points:

- A split-beam scientific echo sounder is used to profile methane bubble plumes
- Repeat observations suggest order-of-magnitude gas flow variability over hours
- One third of known seep sites in the survey area are detected during each pass

Supporting Information:

- ms_similarity_data

Correspondence to:

K. Jerram,
kjerram@ccom.unh.edu

Citation:

Jerram, K., T. C. Weber, and J. Beaudoin (2015), Split-beam echo sounder observations of natural methane seep variability in the northern Gulf of Mexico, *Geochem. Geophys. Geosyst.*, *16*, 736–750, doi:10.1002/2014GC005429.

Received 13 JUN 2014

Accepted 21 JAN 2015

Accepted article online 28 JAN 2015

Published online 19 MAR 2015

Abstract A method for positioning and characterizing plumes of bubbles from marine gas seeps using an 18 kHz scientific split-beam echo sounder (SBES) was developed and applied to acoustic observations of plumes of presumed methane gas bubbles originating at approximately 1400 m depth in the northern Gulf of Mexico. A total of 161 plume observations from 27 repeat surveys were grouped by proximity into 35 clusters of gas vent positions on the seafloor. Profiles of acoustic target strength per vertical meter of plume height were calculated with compensation for both the SBES beam pattern and the geometry of plume ensonification. These profiles were used as indicators of the relative fluxes and fates of gas bubbles acoustically observable at 18 kHz and showed significant variability between repeat observations at time intervals of 1 h–7.5 months. Active gas venting was observed during approximately one third of the survey passes at each cluster. While gas flux is not estimated directly in this study owing to lack of bubble size distribution data, repeat surveys at active seep sites showed variations in acoustic response that suggest relative changes in gas flux of up to 1 order of magnitude over time scales of hours. The minimum depths of acoustic plume observations at 18 kHz averaged 875 m and frequently coincided with increased amplitudes of acoustic returns in layers of biological scatterers, suggesting acoustic masking of the gas bubble plumes in these layers. Minimum plume depth estimates were limited by the SBES field of view in only five instances.

1. Introduction

Marine methane gas seeps support diverse biological communities on the seafloor; indicate locations of potentially exploitable hydrocarbon deposits; increase localized concentrations of dissolved methane in the water column; and, in cases of free gas ebullition and bubble ascent through the water column, may contribute directly to the atmospheric quantity of this potent greenhouse gas [Judd, 2003, 2004; Greinert and Nützel, 2004; Hovland *et al.*, 2012; Mienert, 2012]. Accordingly, interest from public, scientific, environmental, and governmental groups in marine methane gas seeps has increased significantly in recent decades [Judd *et al.*, 2002; Hovland *et al.*, 2012]. Of widespread and long-term interest are the locations of gas vent areas, the quantities and fates of free gas bubbles in the water column, and the variability of seep activity at sites of active venting such that long-term averages of gas flux can be estimated [Naudts *et al.*, 2006; Greinert, 2008; Hovland *et al.*, 2012; Kannberg *et al.*, 2013]. In this study, we present a method for georeferencing and characterizing the acoustic responses of natural marine gas bubble plumes observed with a widely installed fishery research echo sounder. This method is capable of positioning gas vent areas on the seafloor with accuracies near those of a multibeam echo sounder used for bathymetric mapping. The acoustic scattering strengths of plumes are compared after isolation from effects of the observational platform and environment, such as the echo sounder pulse length and orientation as well as the plume shape due to currents. This method is employed to identify and to evaluate the temporal variability of gas vent sites during two series of ship-based acoustic surveys in the northern Gulf of Mexico in 2011 and 2012.

1.1. Acoustic Observations of Marine Gas Bubbles

Ship-based acoustic methods have been demonstrated to be suitable for detecting midwater plumes of gas bubbles [e.g., Greinert *et al.*, 2006], locating corresponding vent sites on the seafloor [e.g., Artemov, 2006], and estimating the shallowest depths of bubble survival. Acoustic methods offer advantages over gas flux measurement systems requiring in situ bubble monitoring or collection equipment [e.g., Hornafius *et al.*, 1999] in that echo sounders may be readily applied over large spatial scales and do not affect gas or water flow at the seafloor [Judd, 2003]. Natural methane seeps have been detected and investigated with acoustic

techniques in every major ocean on Earth [Judd, 2003] using various combinations of split-beam scientific echo sounders (SBES) [e.g., Naudts et al., 2006; Weber et al., 2012a], multibeam echo sounders (MBES) [Nikolovska et al., 2008; Weber et al., 2012c], side-scan sonars [e.g., Jones et al., 2010], subbottom profilers [e.g., Naudts et al., 2006], and acoustic Doppler current profilers [e.g., Holland et al., 2006]. SBES systems have also been used for detecting and monitoring anthropogenic seeps including methane gas and oil released into the water column from leaking wells and pipelines [Johansen et al., 2003; Hickman et al., 2012; Weber et al., 2012b]. While the source of gas on the seafloor might truly include many small point sources, we are limited (as in all investigations) in the resolution of the instrument. In this study, we consider a seep or gas vent to be a region on the seafloor that produces a plume of gas bubbles occupying a small range of target angles (angles from the sonar to the acoustic scatterer of interest) within the larger echo sounder field of view at each range. That is, the horizontal extent of the train of bubbles near the seafloor is approximately an order of magnitude smaller than the beam width footprint at that depth. Several terms are used in the literature to describe acoustic observations of bubbles in the water column, including “flares,” “seeps,” and “plumes.” In this study, the phrase “plume observation” refers to acoustic data indicating a train of free gas bubbles ascending through the water column from a seep area on the seafloor.

In this study, an 18 kHz Simrad EK60 SBES was utilized for detection, georeferencing, and target strength (TS) characterization of marine gas seeps in the northern Gulf of Mexico. SBES systems have been traditionally employed in fishery research, for which standard methods of in situ beam pattern measurements have been developed that enable calibrated TS measurements [Foote et al., 1987]. Calibrated TS measurements for gas bubbles are necessary to accurately calculate the bubbles’ acoustic scattering cross sections, which depend primarily on gas composition, bubble radius, and ambient conditions [Clay and Medwin, 1977]. Given information or assumptions about gas composition, distribution of bubble radii, and ambient conditions, calibrated TS measurements facilitate calculation or estimation of gas flux [e.g., Artemov et al., 2007; Ostrovsky et al., 2008; Weber et al., 2014]. Though no estimates of gas flux are made in this study owing to the lack of direct bubble composition and size distribution data, the calibrated TS measurements possible with SBES systems represent a significant advantage over noncalibrated echo sounders for this purpose where bubble composition and size distribution data are available.

Some of the advantages of using a SBES for seep investigation were identified by Artemov [2006] and addressed in part for studies with a Simrad EK500, a precursor to the EK60, in the Black Sea. The method described herein is similar to that described by Artemov [2006] but also incorporates several distinct features with regard to georeferencing seep targets, characterizing the scattering strength profiles of plumes, and establishing the limits of the echo sounder field of view (FOV). This method was applied to data collected during repeat surveys in an area of active venting in 2011 and 2012 (Figure 1) to evaluate the variability in acoustic scattering strengths of gas bubbles and bubble fates, including the presence and absence of plumes with consideration for the echo sounder FOV. These factors have significant implications for long-term average flux estimates. While variability has been studied previously [e.g., Leifer et al., 2004; Greinert, 2008; Schneider von Deimling et al., 2011], this study adds to the body of research by examining variability in gas flow over a relatively large region (8 km survey lines with an approximately 290 m diameter echo sounder footprint on the seafloor) during repeat survey passes spanning a comparatively long-time scale (up to 7.5 months). The results of this study confirm the applicability of SBES systems for georeferencing of seep sites and calibrated TS monitoring for gas flow, and also demonstrate acceptable gas vent positioning accuracy with the SBES compared to MBES. Calibrated TS data are further compensated in this study for the effects of echo sounder pulse length, vessel orientation, and plume axis deformation due to currents; the resulting scattering strength is normalized by the vertical extent of plume ensonification and referred to as S_z , z being the vertical axis of interest for bubble transport. For a given frequency, S_z facilitates unbiased comparison of plume scattering strengths along the vertical axis across observational platforms (e.g., different echo sounder pulse lengths and orientations) and environmental conditions (e.g., currents which deform the plumes during ascent). These factors are not considered completely in other scattering strength values used in the literature, such as volume scattering (S_v), area scattering (S_a), or TS. For instance, holding all other parameters constant, a change in echo sounder pulse length from 1 to 4 ms between surveys would result in a 6 dB increase in TS. Of interest for future seep mapping efforts, our observations show large variability in plume presence and scattering strength, suggesting that long-term flux estimates in the Gulf of Mexico would benefit from repeat surveys because single-pass surveys do not identify all vent

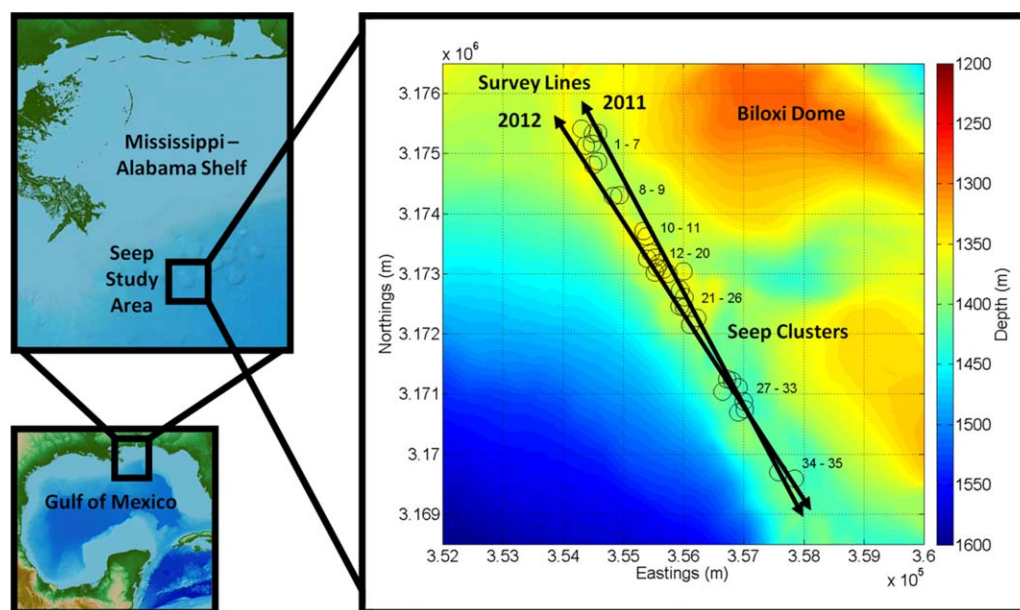


Figure 1. Seep study area on the southwest edge of the Biloxi Dome in the northern Gulf of Mexico. Projection is Universal Transverse Mercator (UTM, zone 16 North) referenced to the WGS84 ellipsoid. Bathymetric data were collected with a 30 kHz Kongsberg EM302 MBES aboard NOAA Ship *Okeanos Explorer* during SBES data collection in 2011. The survey lines represent the mean ship tracks during data collection in 2011 and 2012. Clusters are numbered sequentially from northwest to southeast and indicated by circles with radii of 145 m to represent the approximate SBES beam width footprint on the seafloor. Circles are centered at the means of seep positions for each cluster. Gulf of Mexico maps on left adapted from NOAA image (http://www.ngdc.noaa.gov/mgg/image/gom_hillshade.jpg).

sites along a survey track line, capture the variability in plume scattering strengths at known vent sites, or establish relationships in gas flow between nearby vent sites which may be linked by subbottom gas migration pathways.

2. Methods

An 18 kHz Simrad EK60 SBES with 4 ms transmit pulse length and one-way -3 dB total angular beam width of 12° was used to collect water column backscatter data during repeat seep mapping surveys aboard NOAA ship *Okeanos Explorer* over the southwest edge of the Biloxi Dome in the northern Gulf of Mexico (Figure 1), a region well known for gas venting [Judd *et al.*, 2002; MacDonald *et al.*, 2003; Weber *et al.*, 2014]. Unless specified otherwise, all echo sounder descriptions and data discussed in this text refer to the Simrad EK60 SBES and the FOV refers to the 12° cone representing the echo sounder beam width. The transducer was mounted adjacent to the vessel's Kongsberg EM302 MBES on a hull "blister" designed for acoustic sensors at approximately 4.6 m depth. Data collected include echo strength (apparent target strength prior to compensation for transducer beam pattern) and digitized electrical phase differences in the alongship (bow-to-stern) and athwartship (port-to-starboard) directions (Figure 2). Vessel position and attitude were measured with an Applanix POS/MV 320 motion sensor receiving position corrections from a C-NAV 2050 differential global positioning system (GPS), yielding position and attitude uncertainties of 1.3 m (horizontal dilution of precision) and 0.02° (one standard deviation), respectively.

Twenty-seven acoustic survey passes over the Biloxi Dome were conducted on NNW and SSE headings in late August and early September 2011 and April 2012 (Figure 1 and supporting information Table S1). Time intervals between passes varied from less than an hour to over a week during the 2011 survey. Survey operations in 2012 were broken into two sessions separated by approximately 12 h, with mean time intervals between survey passes of 1.2 and 1.7 h for the first and second sessions, respectively. In order to improve coverage of known vent sites during the 2012 survey, the mean survey orientation (course over ground) was adjusted from 152° – 332° in 2011 to 147° – 327° in 2012. Additionally, to increase the number of pings containing plume data at each known vent site, mean vessel speed during survey operations was reduced from 11.3 kn in 2011 to 10.0 kn and 7.0 kn during the first and second sessions, respectively, in 2012. Survey

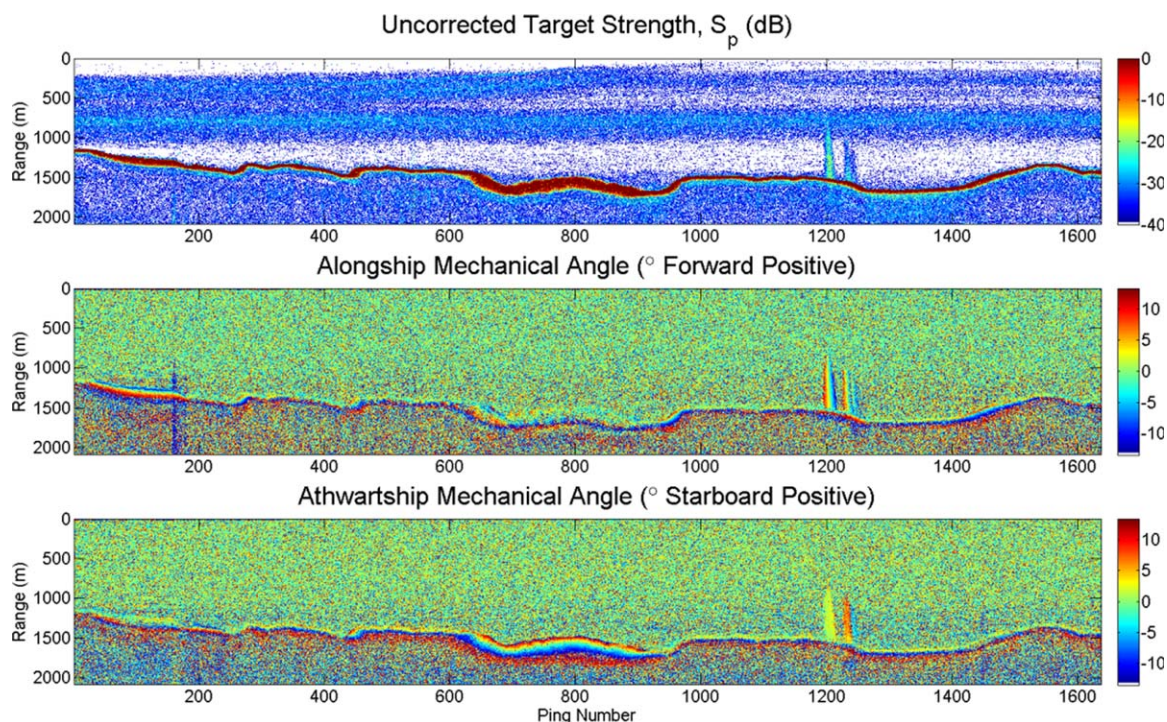


Figure 2. SBES data collected during seep investigation included echo strength (apparent TS before correction for transducer beam pattern, top) and mechanical target angles in the alongship (middle) and athwartship (bottom) directions. Data are plotted versus range (vertical axis) and ping number (horizontal axis). Example data include interference (near ping 175) and two seep observations (near pings 1200 and 1250). Each seep observation is characterized by anomalously high scattering strength (blue to light blue, top), progression of alongship target angles from ahead to astern (red to blue, middle), and small changes in athwartship target angle (nearly constant color, bottom). The seafloor varies between 1200 and 1700 m in this example. Two scattering layers are visible in the echo strength data: one deeper scattering layer at a range of approximately 750 m and one shallower scattering layer which migrates upward from approximately 500–250 m between ping numbers 400–1000 (corresponding to sunset and dusk between approximately 0000–0100 GMT, or 1900–2000 local time).

pass details are available in supporting information (Table S1), with an example of ship tracks near a cluster of gas vent positions (supporting information Figure S1).

The sound speed at the depth of the transducer was measured continuously throughout both surveys at a sample rate of 10 Hz and used to convert target electrical phase differences to mechanical angles in the transducer reference frame. Sound speed profiles were measured using expendable bathythermograph (XBT) probes at intervals of approximately 8 h during 2011 and 6 h during 2012. Salinity data were derived from conductivity, temperature, and depth (CTD) profiles collected at multiple locations during both cruises. Acoustic absorption profiles were calculated from temperature, salinity, and depth data using the Francois and Garrison model with an estimated pH of 8.0 [Francois and Garrison, 1982a, 1982b]. All data were processed using sound speed and absorption profiles derived from XBT and CTD measurements nearest in time. Sound speed profiles applied to SBES data in this study are available in supporting information (supporting information Figure S10).

Raw data were parsed with freely available software [Towler, 2010], after which all further processing was completed using MATLAB scripts developed for this study; while the scripts are not intended for publication, a process diagram of the steps implemented in MATLAB for each plume observation is presented in supporting information Figure S8. Each data file was visually scrutinized for plume observations, each characterized by a vertically oriented region of elevated scattering strength corresponding with a fore-aft trend in alongship target angle and highly consistent athwartship target angle (Figure 2). For each plume observation, an ambient scattering strength profile was calculated using at least 30 of the nearest pings not containing plume targets; this is referred to as the “noise” profile. To eliminate bottom returns and weak scatterers from further processing of plume observations, the data were threshold-filtered to exclude those with echo strength outside the range of -40 to 0 dB (based on thresholds applied for visual identification of plumes) and signal-to-noise ratio less than 10 dB. Corrections for vessel position, vessel attitude,

orientation of the transducer in the vessel reference frame, and refraction of the acoustic raypath were applied to georeference all threshold-filtered plume targets. These georeferenced plume targets were then used to estimate the associated gas vent positions on the seafloor, calculate plume TS profiles, and estimate the minimum depths reached by bubbles acoustically observable at 18 kHz. More detailed descriptions of the methods for TS calibration, target positioning, timing corrections, and determination of transducer angular offsets are available in supporting information S1.1–S1.4.

2.1. Seep Clustering

To identify repeat observations of unique seep sites across surveys, plume observations were grouped by finding clusters of their associated gas vent position estimates in which all were separated by no more than a given “linking distance” of 65 m from at least one other gas vent. The linking distance approximates the largest expected horizontal positioning uncertainty in the survey area according to the split-aperture correlation method employed by the echo sounder for target angle calculation (supporting information S1.5). This linking method relies on georeferenced plume data in the water column to identify spatial relationships among gas vent areas on the seafloor; accordingly, even if linked by subbottom gas migration pathways, seep sites separated by more than 65 m may be treated as separate clusters using this criterion.

Based on simultaneous 2011 multibeam echo sounder observations, in which plumes near nadir typically subtended angles far less than the SBES beam width, each seep site was expected to have an areal extent much smaller than the SBES beam width footprint on the seafloor (approximately 290 m diameter at 1400 m depth). Because no seep sites were observed in 2011 with areal extents exceeding the split-beam echo sounder beam width footprint (which would be termed “diffuse” seeps in the view of this echo sounder), every plume observation was expected to capture the entire areal extent of the associated gas venting area on the seafloor. Plumes from gas vent areas of this nature occupy less than the beam width-limited ensonified volume and are hereafter described as “discrete” plumes in this study.

2.2. TS of Seep Targets

Midwater gas bubbles of radii much smaller than the acoustic wavelength scatter incident acoustic energy isotropically by damped harmonic oscillation (supporting information S1.6). Figure S2 (supporting information) presents the frequency and radius dependencies of TS for single bubbles of free methane gas in seawater; in this figure, bubble resonance conditions are characterized by a TS peak for each bubble radius. The smaller radii used in this example (1–5 mm) are representative of methane gas bubbles observed using remotely operated vehicles equipped with high-definition cameras and visual bubble sizing apparatus during the 2012 data collection period in the vicinity of the study area [Weber *et al.*, 2014] and by other marine gas investigations in the Gulf of Mexico [Leifer and MacDonald, 2003] and at other deep water gas vent sites in the Barents Sea [Sauter *et al.*, 2006], Black Sea [Sahling *et al.*, 2009], and Arabian Sea [Römer *et al.*, 2012]. Based on the depth and radius dependencies of TS for methane bubbles depicted in Figure S2, it is expected that changes in TS profiles represent changes to parameters of the ensonified bubbles acoustically observable at 18 kHz. For instance, changes in TS during bubble ascent may reflect changes in the numbers of bubbles acoustically observable at 18 kHz, changes in the bubble size distribution, changes in the scattering strengths of acoustically observable bubbles, or a combination thereof. Without knowledge of the bubble size distribution in an ensonified target volume, ambiguity exists in the relationship between TS at any single frequency and the total volume of gas ensonified.

2.3. S_z for Single Discrete Plumes

Though gas flux estimation is not possible for bubbles ensonified at a single frequency without knowledge of bubble size distribution, temporal variability in scattering strength may be indicative of relative changes in gas flux for a single source with constant bubble size distribution. Likewise, scattering strength variability along a plume axis in the vertical direction may indicate changes to net vertical gas flux and bubble behavior or survival during ascent [e.g., Rehder *et al.*, 2002; McGinnis *et al.*, 2006]. However, TS does not account for the geometry of intersection between the transmit pulse and the plume axis. This geometry of intersection directly affects the number of bubbles ensonified for a given plume and depends on transmit pulse length, echo sounder orientation, and depth-dependent plume deformation due to water current structure. These parameters vary significantly between plume observations and among echo sounder configurations for seep studies. To isolate a scattering strength value independent from these variations, a quantity, S_z (dB re 1 m^{-1}) describing TS per unit of vertical extent of plume ensonification is suggested as

$$S_z = TS - 10 \log_{10} dz, \quad (1)$$

where dz is the vertical extent (m) of plume axis ensonification (supporting information Figure S3). The inherent assumption in this definition is that the range of target angles subtended by a discrete plume is small compared to the beam width, as required for split-aperture target angle calculation. Further, TS is normalized by the vertical extent of the plume within each sample because it is assumed that the vertical flux of gas is the quantity of interest. From Figure S3, dz is calculated as

$$dz = L \cos \theta, \quad (2)$$

where L is the length of intersection between the transmit pulse and the plume axis. Angle θ is measured from vertical to the plume axis unit vector, \vec{u}_p , along which all bubbles are assumed to have the same direction of ascent. L is calculated as

$$L = \frac{c\tau}{2 \cos \phi}, \quad (3)$$

where c is sound speed (m/s) at the target estimated from sound speed profile data and τ is the transmit pulse length (s). ϕ is the angle between \vec{u}_p and \vec{u}_r calculated from the dot product definition

$$\cos \phi = \frac{\vec{u}_r \cdot \vec{u}_p}{|\vec{u}_r| |\vec{u}_p|}, \quad (4)$$

where \vec{u}_r is the unit vector aligned with the refraction-corrected path of the incident planar acoustic wave. For observations of single discrete plumes, the quantity S_z isolates TS from effects of transducer orientation, plume deformation, and changes in pulse length to facilitate comparison of acoustic scattering strengths of bubbles along the vertical dimension of interest for gas flux. Figure 3 compares TS and S_z profiles for a single plume observation, showing a fairly consistent difference between the profile amplitudes. The apparent consistency of the difference between TS and S_z in this example is due to the relatively uniform vertical orientations of the echo sounder and plume axes and the single transmission pulse length (4 ms) used in this study. As S_z normalizes TS for the effects of these survey parameters to facilitate comparison of scattering strengths across studies, the difference between TS and S_z would be expected to vary for other survey configurations and plume orientations.

2.4. Diffuse and Multiple Discrete Plumes

Characterization of relative gas flux by S_z is appropriate for single discrete plume observations, as the collective backscattering strength for a single stream of bubbles in each echo sounder sample volume is expected to be the only significant contributor to TS at each sample range. Because the beam pattern compensation for TS calculation depends on accurate target angle calculation, which is confounded by the presence of strong scatterers at different target angles at each range, observations of multiple discrete plumes or diffuse plumes within the echo sounder field of view are likely plagued by erroneous target positioning, TS correction, and S_z calculation.

The single discrete natures of plumes were verified using simultaneous multibeam echo sounder data processed in the commercial water column mapping software QPS Fledermaus FMMidwater (supporting information Figure S4); any multiple discrete or diffuse plumes apparent in the multibeam data that also fell within the split-beam echo sounder field of view were flagged during further analyses (Figure 5, double exclamation points). In studies where simultaneous multibeam data are not available, identification of diffuse or multiple discrete plumes is problematic. It may be possible to identify the presence of diffuse plumes by examining the coherence of the target angle data, but this possibility was not explored here. In cases of diffuse plumes, volume scattering strength (S_v) is a more appropriate measure of collective scattering strength for randomly spaced, noninteracting bubbles [Clay and Medwin, 1977].

3. Results

3.1. Seep Observations and Positions

To identify repeat observations of unique seep sites at similar locations throughout the study area, seep area position estimates calculated from SBES plume data were grouped (or “clustered”) using a linking distance of 65 m. This method yielded 35 clusters (Figure 1 and supporting information Table S2), each

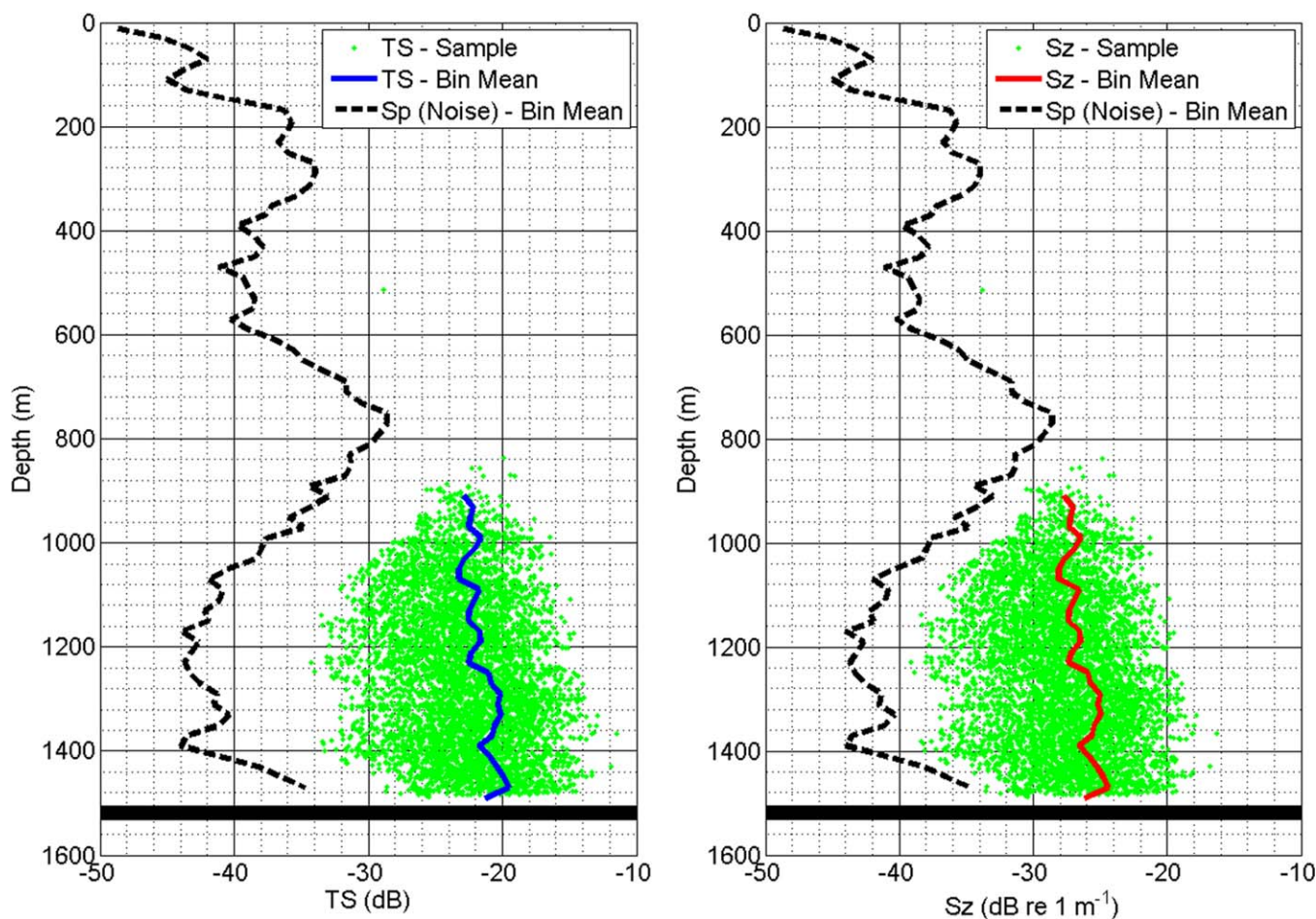


Figure 3. TS and S_z profiles for an example SBES plume observation (Figure 2, near ping 1200). Dashed lines are noise profiles based on 30 pings immediately neighboring the plume observation. Green points represent scattering strengths of targets after threshold-filtering to exclude the seafloor (thick black horizontal line) and very weak scatterers, as well as for minimum signal-to-noise ratio of 10 dB. Each profile is constructed from binned data with depth bin widths of 20 m and a minimum count of 10 samples. The TS and S_z profiles share similar shapes with approximately a 5 dB difference. This consistency stems from normalization for vertical extent of plume ensonification of approximately 5 dB for all samples based on the fixed echo sounder pulse length and near-vertical plume and echo sounder orientations. TS would have likely shown more variation with increased plume deformation or changing echo sounder configuration. The intent of S_z calculation is to isolate TS (and changes in TS) from effects on scattering strength related to the observational platform (echo sounder configuration and vessel motion) as well as plume deformation such as that which may result from currents.

including between 1 and 25 SBES observations on repeat survey lines, with a total of 161 seep area position estimates among all clusters. Additional cluster data are available in supporting information Table S2. For each cluster, the mean of SBES gas vent position estimates was taken as the cluster center. Nine clusters contained SBES observations from both 2011 and 2012, whereas eight clusters contained only 2011 data and 18 clusters contained only 2012 data. These differences in plume counts per cluster between years are related primarily to realignment of the survey track line from 2011 to 2012. Among clusters containing two or more plume observations, the horizontal differences between estimated gas vent positions and cluster centers on the seafloor averaged 35 m with a standard deviation of 19 m.

To examine the SBES seep positioning accuracy, SBES gas vent position estimates were compared to “benchmark” positions from simultaneous MBES observations in 2011 (supporting information Figure S5). Results suggest SBES seep positioning accuracy on the order of MBES positioning capability for most cases of single discrete plumes. Additional information regarding SBES gas vent positioning results relative to MBES benchmarks is available in supporting information S2.1.

3.2. S_z Profiles and Plume Depths

Profiles of S_z versus depth were created for all plume observations (supporting information S2.2). The minimum acoustically observable plume depth was estimated for every plume observation by visual scrutiny of

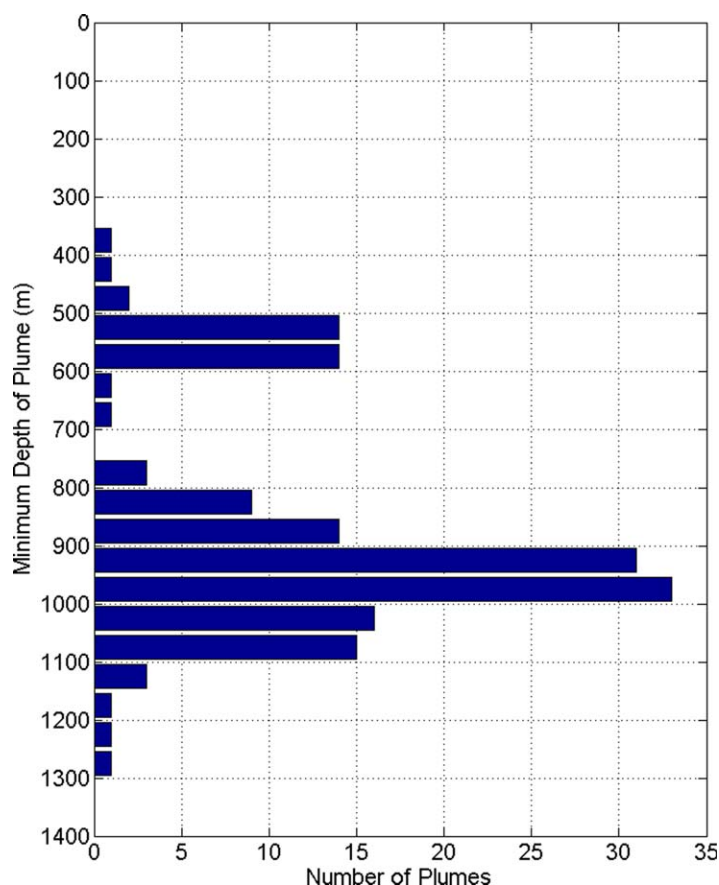


Figure 4. Distribution of minimum plume depths observed acoustically at 18 kHz based on manual scrutiny of echo strength and trends in alongship and athwartship mechanical angles. Of 161 plumes originating at approximately 1400 m depth in the seep study area, 156 appeared to terminate within the echo sounder FOV. Minimum depth estimates fell outside the echo sounder FOV on five occasions and were likely limited (or “cutoff”) by the echo sounder FOV. Four of these five minimum observed plume depths fell between 1000 and 1200 m and one was estimated at approximately 550 m.

18 kHz into a bimodal distribution, with 34 plumes (21% of all observations) appearing to extend shallower than 700 m and the remainder appearing to terminate deeper than 750 m (Figure 4); no estimates fell between 700 and 750 m. This dividing effect of the deep scattering layer contributes to the relatively large standard deviation of 191 m among all estimates of the shallowest depths attained by bubbles acoustically observable at 18 kHz. Importantly, the bubble plumes detected in this study may have physically reached shallower waters than the minimum depths observed in the acoustic data collected at a single frequency; in these cases, ensonification at other frequencies (perhaps closer to the frequency of bubble resonance) may have yielded different estimates of the minimum depths of acoustically observable bubbles [e.g., *Greinert et al.*, 2010]. Limitations of the SBES FOV did not appear to impact a significant portion of minimum plume depth estimates. Of 161 plume observations, 156 (97%) were observed to terminate within the SBES FOV and five were likely “cutoff” by the FOV. Four of the five FOV-limited minimum plume depth estimates fell within the depth range of 1020–1200 m, with one estimate at 550 m.

Mean S_z values were calculated from all targets in the deepest 200 m of each plume observation for relative comparison of temporal changes of gas flow activity at the gas vent sites, including apparent starting and stopping of bubble release acoustically observable at 18 kHz (Figure 5). The depth range of the deepest 200 m of plume targets was selected to include targets in the 10 S_z profile depth bins nearest the seafloor; each depth bin has a width of 20 m to achieve a typical count of at least 10 samples in each bin. Mean S_z values in the deepest 200 m were calculated for all but one observation, at which the S_z profile contained insufficient data for averaging in the deepest 200 m (“X,” Figure 5). In one case, two separate SBES plume

TS and target angle data, yielding minimum plume depth estimates with a mean of 875 m. The shallowest observed plume depth was approximately 360 m, with 32 plumes (20% of all observations) rising to depths shallower than 600 m (Figure 4). Most acoustic plume observations appeared to terminate below 600–800 m, one of several depth ranges characterized by increased densities of biological acoustic scatterers known collectively as the “deep scattering layer” [*Urick*, 1975] (Figures 2, 3, supporting information S4, and supporting information S6). For example, two distinct depth ranges within the deep scattering layer are visible in Figure 2 (top), with two plume observations appearing to terminate in the deeper layer between 800 and 1200 m depth.

In general, reduced signal-to-noise ratio in the deep scattering layer between 600 and 900 m depth tended to divide the estimated minimum depths of bubble plumes acoustically observable at

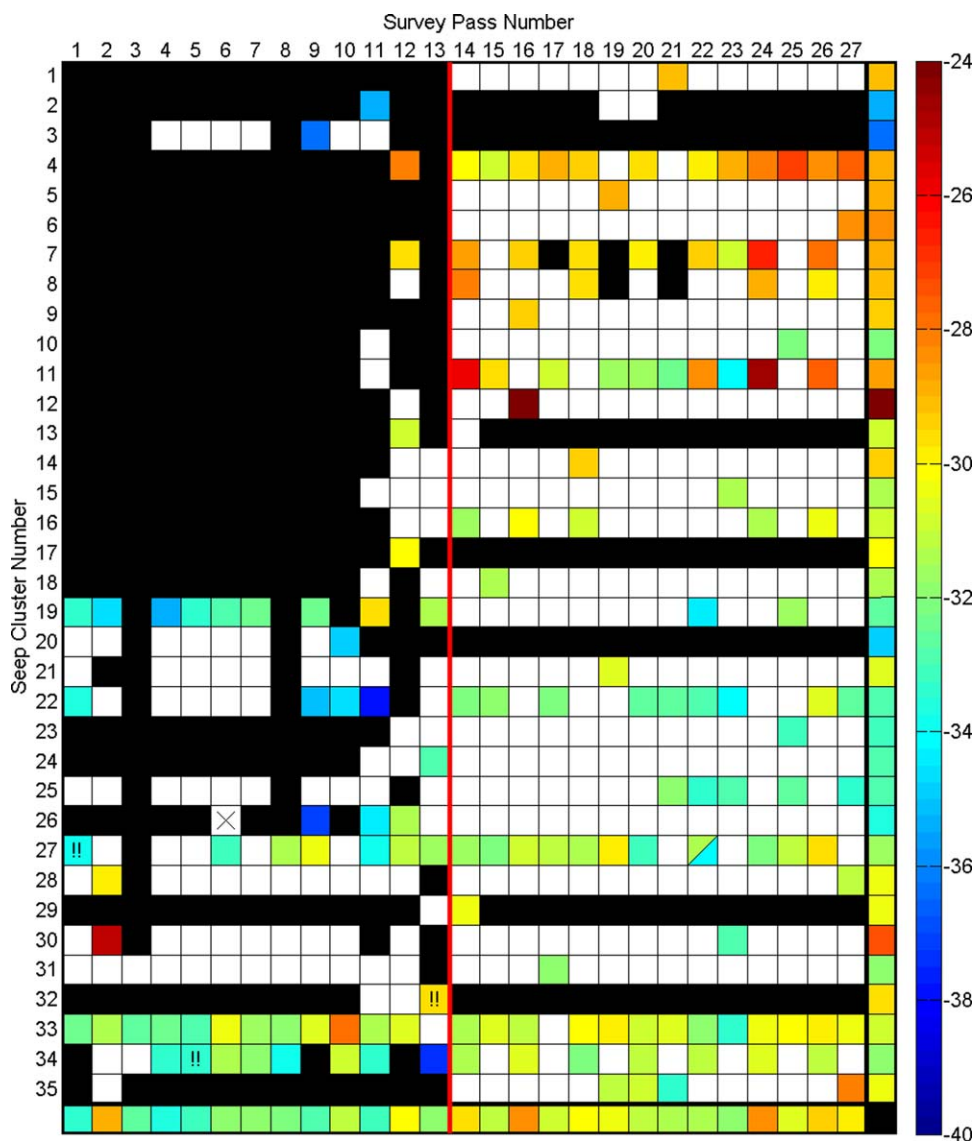


Figure 5. Variability in presence and acoustic scattering strength of plume observations at cluster locations over surveys in 2011 and 2012. Survey pass times are listed in Table S1. Color represents the mean S_2 in the deepest 200 m. White indicates that the cluster position was expected to pass within the echo sounder field of view but no plume was observed; black indicates passes during which the cluster position was not expected to be visible due to ship position and orientation of the echo sounder field of view. In one instance, two separate seep observations on a single survey pass (22) satisfied the cluster linking distance criterion and were associated with the same cluster 27; these observations are represented by a split cell with the upper and lower triangle colors pertaining to the first and second seep observations, respectively. The "X" for cluster 26 during pass 6 indicates that a seep was observed but the S_2 profile contained insufficient data for calculation of mean S_2 in the deepest 200 m. For the 55 SBES plume observations in 2011, MBES data suggest that two distinct plumes are included within the SBES FOV on three occasions; these instances are marked by double exclamation points. 2012 MBES data have not been reviewed for similar instances. Means of the plotted values for each cluster and each survey pass are shown in the right column and bottom row, respectively.

observations during one survey pass satisfied the seep clustering proximity criterion and were assigned to a unique cluster; Figure 5 includes both mean S_2 values in the deepest 200 m as a diagonally split cell. Coverage for the echo sounder FOV on the seafloor was estimated for each survey pass to determine whether a plume at each cluster position would have fallen inside or outside the horizontal range of plume positions expected to be visible. In cases of no plume observation within a cluster during a survey pass, an indication is made in Figure 5 for whether the cluster position fell within the echo sounder FOV on the seafloor and was expected to be visible. Means of plotted values for each cluster across all passes and each pass across all clusters are plotted on the right side and bottom of Figure 5, respectively.

4. Discussion

4.1. Seep Positioning and Clustering

For seep areas separated by more than the SBES beam width footprint on the seafloor, the development and application of processing steps for georeferencing plume targets observed with the SBES has been shown to yield seep positioning accuracy commensurate with that of the MBES calibrated for bathymetric and midwater mapping used in this study. These results suggest that plumes detected with SBES and traced to similar seafloor positions correspond to repeat observations of unique seep areas within the positioning resolution of the SBES, thus facilitating comparison of scattering strength profiles based on repeat measurements of calibrated TS for plumes originating at unique seep areas on the seafloor. Likewise, barring other factors which may inhibit the detection of plumes, such as excessive ship noise or interference from other echo sounders, the SBES positioning capability demonstrated here increases confidence in the conclusions of absence of bubbles acoustically observable at 18 kHz when the echo sounder FOV includes a known seep site but no plume is observed.

Though plumes were observed repeatedly during survey passes conducted on two narrow ranges of headings (NNW and SSE), MBES gas vent position benchmarks are distributed in all directions relative to simultaneous SBES position estimates. The MBES and SBES gas vent positions typically differ by an order of magnitude less than the SBES footprint diameter (Figure S5). These results suggest that the erroneous SBES timing data and unknown SBES transducer angular offsets, the most likely contributors to large and systemic positioning errors have been substantially resolved. Timing correction and angular offset estimation appear to be practical and worthwhile steps for georeferencing SBES data in future studies.

The disadvantages of seep positioning with SBES are related to beam width and availability of target angle data within the beam width-limited FOV. Of primary consequence, the SBES beam width of 12° provided limited athwartship FOV coverage compared to MBES. Second, the ability to distinguish among separate plumes rising simultaneously within the FOV is limited by the SBES split-aperture correlation method, which produced one pair of alongship and athwartship target angles per range sample per transmit-receive cycle (e.g., Figure 2). This second concern of coincident echoes from separate plumes may be addressed in future studies by closer examination of target angle data which cannot be readily distinguished visually. For instance, data selected for a plume observation may contain threshold-filtered targets associated with multiple plumes originating from distinct seep areas on the seafloor. This causes difficulties in target angle estimation using split-aperture correlation, which is based on an assumption of a single target at any given range. No attempt was made in this study to examine changes in target angle data trends between single discrete, multiple discrete, and diffuse seep sites. All threshold-filtered targets within each SBES plume observation were attributed to a single-seep location, limiting the distinction of discrete gas vent areas falling within the SBES beam width and requiring scrutiny of MBES data to identify instances of multiple plumes. MBES data from 2011 showed two distinct plumes for 3 out of the 55 concurrent SBES plume observations, suggesting that the assumption of contributions from a single gas vent area to SBES TS data and target angle measurements is applicable to the large majority of plume observations.

Plume observations were clustered for evaluation of temporal variability based on the proximities of their estimated seep site locations to each other within the SBES horizontal positioning uncertainty of 65 m for a single plume target passing the minimum signal-to-noise ratio threshold filter. The resulting cluster locations were typically separated by at least several hundred meters (Figure 1) and the horizontal distribution of seep area positions in each cluster typically spanned no more than the SBES beam width footprint on the seafloor. As expected for clusters of distinct seep sites, a maximum of one plume observation per survey pass was made at each cluster during almost all passes. On only one occasion, two unique plumes and their associated distinct seep position estimates observed on a single pass were later assigned to the same cluster. This "dual-seep" observation was recognized as an artifact of the clustering method, which otherwise succeeded in identifying and assigning a maximum of one plume observation per pass to each cluster based on proximity alone. It is important to note that cluster boundaries had no typical shape, as the linking distance had no directional component and was applied with the sole intent of grouping seep area position estimates by proximity. The absence of any general trends in cluster shapes suggests that seep locations were not consistently distributed within each cluster. This distribution of seep positions within a cluster

may be a result of random measurement error, changes in the activities of closely spaced but separate bubble sources on the seafloor, or a combination of these factors.

Clustering of plume observations was performed based on proximity of estimated seep locations on the seafloor within the maximum expected split-beam echo sounder horizontal positioning uncertainty of 65 m in 1400 m water depth. However, the results of this method may not have completely captured the geological links between gas vent sites. For instance, though identified and isolated as distinct clusters by the linking distance of 65 m, several of the 20 clusters containing only one seep area lend themselves to consideration alongside other nearby clusters that also contained one or more seeps. This is evident primarily where the clustering process has produced multiseep clusters that are extended in the along-track direction but excluded nearby isolated seep areas that did not meet the linking distance criterion. For example, single-seep cluster 5 falls within the along-track extent of multiseep cluster 4, which itself has a distribution of seep positions roughly equal to the separation between clusters 4 and 5 (approximately 120 m, or less than the SBES beam width footprint radius at 1400 m). The single seep observation in cluster 5 was made during pass 19, corresponding with plume absence in cluster 4 and raising the possibility that plume observations in clusters 4 and 5 are related and may originate from the same subbottom network of gas migration pathways belonging to one broad seep area. Similar consideration may be applied for the pairs of single-seep clusters 6 and 9 with multiseep clusters 7 and 8, respectively. There are also instances of closely spaced but distinctly numbered multiseep clusters containing plume observations which may be related. For example, cluster 27 contains 19 seeps which satisfy the linking distance criterion but are spread along track over approximately 250 m. This along-track distance overlaps that of cluster 28, which is centered less than 100 m from the center of cluster 27 and includes two plumes observed on passes with no observations at cluster 27. Though these clusters were identified and separated based on proximity of individual seep observations, the spacing and timing of those observations suggest that gas vents in clusters 27 and 28 are closely related. These examples raise the possibility that the simple linking distance clustering method may not adequately capture temporal relationships between nearby seep sites and may yield cluster dimensions much larger than the beam width footprint. Additional consideration for the timing of seep observations in close proximity during the clustering process may prove useful in grouping vent sites which exhibit related gas flow even if physically separated by more than the linking distance. Likewise, timing criteria would aid in delineating among seep areas which satisfy a given proximity criterion but are not related in their flow behaviors. In this study, the linking distance of 65 m was applied as a simple grouping criterion and generally produced well-separated clusters containing one repeat plume observation per pass. This method could be readily applied to future seep studies, with adjustment of the linking distance appropriate for the echo sounder beam width.

4.2. Plume Observations and S_2 Profiles

The SBES FOV coverage of clusters 1, 4–12, 14–16, 18, 23–24, 26, and 35 was limited during 2011 due to alignment of the survey track line, which was adjusted by approximately 5° heading in 2012 to provide more consistent coverage of all clusters (Figure 1). Clusters 2–3, 13, 17, 29, and 32 included only single seep position estimates in locations that fell just beyond the expected FOV coverage for most passes during both surveys; as such, coverage did not improve at these clusters from 2011 to 2012. Despite the survey track line realignment and associated change in FOV coverage, no appreciable difference was noted between 2011 and 2012 in the variability of plume observation rates. For instance, the ratio of total plume observations to number of cluster locations within the echo sounder FOV varied from low ratios of 3:12 (three plumes observed over 12 clusters within the FOV during one pass) during passes 5 and 7 in 2011 and 5:27 during pass 17 in 2012 to highs of 3:6 and 6:12 during passes 8 and 9 in 2011 and 10:28 in passes 22 in 2012. Per-pass rates of plume observation in 2011 and 2012 averaged 0.35 and 0.27, respectively. These results suggest that an average of approximately one third of known seep areas in this study were observed to be venting gas during any given survey pass and that there was no appreciable change in plume presence across the entire survey area during the 2011 and 2012 data collection periods.

Though a general trend in gas flow activity is not evident for the entire survey area, individual clusters varied widely in the rates of plume observations across all passes within the FOV. These rates ranged from lows of 1:26 (one plume observed at one cluster within the FOV in 26 passes) at cluster 31 and 1:23 at cluster 21 to a high of 25:27 at cluster 33, with each cluster typically falling within the SBES FOV during 2011 and 2012. Average plume observation rates at each cluster, accounting for FOV coverage for all passes,

resembled per-pass rates across all clusters with a mean of 0.31; the standard deviation of 0.29 in rate of plume observation at each cluster reflects the wide variability in total plume observations at each cluster location across surveys. Importantly, there was no single cluster that exhibited gas flow on every survey pass, nor was there any single survey pass which observed plumes at all of the cluster locations. Conversely, no survey pass included zero plume observations. Taken together, these results suggest that the rates of plume observations at clusters falling within the SBES FOV are indicators of plume presence or absence which are independent of survey track line orientation and dependent primarily on the activity of gas venting at each cluster location. These results depend heavily on the SBES seep site positioning method and appropriate consideration of the FOV limitations in identifying observations of plumes originating from similar sources on the seafloor; other acoustic survey platforms or data collection environments may present additional challenges for identifying repeat plume observations.

S_z profiles for plumes observed at cluster 22 (supporting information Figure S7) show that plume observations in the upper water column were significantly limited by reverberation in the deep scattering layer between 600 and 900 m depth. That is, the actual plume may extend upward from the top of the acoustic observation. This limit applied to most plume observations, as evidenced by the sharply decreasing frequency of minimum plume depths in the depth range of 600–900 m (Figure 4). The widespread and consistent reductions of bubbles detectable at 18 kHz at depths shallower than 600 m likely correspond with reductions in bubble size due to gas transfer out of the bubbles during ascent [Rehder *et al.*, 2002; McGinnis *et al.*, 2006]. In these cases, it is possible that the seeps would remain detectable at shallower depths in the water column using different acoustic frequencies [Greinert *et al.*, 2010].

For 32 plume observations, gas transfer out of the bubbles was sufficiently slow to enable survival of bubbles detectable at 18 kHz to depths shallower than 600 m. In one case, a plume reached as shallow as 360 m, though no plume observations extended shallower than this depth. Only one plume observation reaching a depth shallower than 600 m was limited by the echo sounder FOV (at approximately 550 m), suggesting that bubbles which had been consistently acoustically observable at 18 kHz during the 800 m ascent from the seafloor to a depth of 600 m dissipated rapidly over the subsequent 250 m. These observations suggest enhanced survival of bubbles for a small number of plumes, followed by rapid reduction of detectable bubbles at depths shallower than 600 m. Formation of methane hydrate shells on the bubbles has been suggested as a mechanism which may inhibit gas transfer and increase the duration of bubble survival for methane bubbles originating at the depth of the survey area and ascending through the depth range over which methane hydrates are stable [Rehder *et al.*, 2002; Leifer and MacDonald, 2003; Judd, 2004; Greinert *et al.*, 2006; McGinnis *et al.*, 2006; Chen *et al.*, 2014]. The shallow (minimum) depth limit of the hydrate stability zone, above which hydrates will dissociate at shallower depths, typically falls between 500 and 600 m in the Gulf of Mexico [Milkov *et al.*, 2000; Tishchenko *et al.*, 2005; Weber *et al.*, 2014] and is calculated according to Tishchenko *et al.* [2005, equation (24)] at 610 m for a typical temperature–depth profile in the study region. This shallow limit of the hydrate stability zone coincides with the depth range containing most of the shallowest depths of detectable bubble survival during this study, suggesting rapid dissolution of methane gas bubbles after dissociation of their hydrate shells. The acoustic effects of methane hydrate shells on TS for bubbles are areas of active research and were not considered here, apart from this discussion of shallow plume observations related to the reduced dissolution of acoustically observable bubbles during ascent through the hydrate stability zone.

4.3. S_z Base Variability

As shown in Figure 5, a wide range of mean S_z in the deepest 200 m was observed throughout the 2011 and 2012 surveys. Assuming constant distributions of bubble sizes at each cluster (though unlikely for large changes in flux), fluctuations in mean S_z of ± 3 dB re 1 m^{-1} would correspond to doubling or halving, respectively, of the numbers of bubbles per vertical meter. In general, mean S_z values for clusters on the NNW end of the survey line (e.g., clusters 1 and 4–9) appear consistently 2–4 dB re 1 m^{-1} higher than those for clusters closer to the middle of the survey line (e.g., clusters 10–26). Survey pass 12 includes the only 2011 plume observations on the NNW end of the survey line at clusters which were also observed with seeps in 2012; these clusters (4 and 7) show relatively consistent agreement in mean S_z between surveys in 2011 and 2012.

A greater number of plumes were observed during the seven NNW-heading passes (61 plumes) than the seven SSE-heading passes (45 plumes) in 2012. This pattern is most obvious in plume detections at cluster

34 (Figure 5), for which plume presence is directly correlated with ship heading in 2012. The unlikelihood of a correlation between gas flow at a cluster and ship heading suggests a difference between estimated FOV coverage and the practical limits of plume target detection during SBES data processing and threshold filtering. Cluster 34 was investigated as a primary example of possible “false positive FOV coverage” estimates in 2012 (Figure 5, cluster 34, odd-numbered passes 15–27). To investigate FOV coverage at cluster 34, the closest approach of the ship to the cluster center during each pass was calculated for comparison to the FOV footprint on the seafloor. The athwartship FOV coverage differs to port and to starboard due to transducer roll offset and vessel roll, which is affected primarily by vessel loading, wind, and sea state. Except for three passes in 2011 (black boxes, Figure 5), the ship passed within 100 m athwartship of cluster 34 on all passes in 2011 and 2012. These athwartship pass distances fell well within the expected FOV coverage of 160 m in the port direction (the bearing to cluster 34 during NNW-heading survey passes in 2012). This is in agreement with plume observation patterns in this data collection period. During SSE-heading passes in 2012, FOV coverage to starboard was reduced to approximately 100 m by a combination of transducer roll offset and vessel roll (Table S1). Closer comparison of the cluster position relative to FOV coverage during these SSE-heading passes showed that cluster 14 typically fell within 30 m of the limit of the expected FOV coverage, or approximately 1° of the -3 dB beam width.

The FOV was defined in this study by the -3 dB beam width of the SBES, and every plume observation included threshold-filtered targets within this angular range. Plume targets were also frequently detected at angles outside the -3 dB beam width. These targets were not included in TS calculations due to limited beam pattern correction data beyond the -3 dB beam width but suggest capability for plume detection outside the beam width-limited FOV coverage estimate. One related concern would be detection of plumes with targets exclusively outside the -3 dB beam width. In this case, a plume would have been detected but not represented in the seep position estimates or TS calculations. However, the careful visual scrutiny of the TS data echograms (similar to Figures 2 and S6) during plume selection and subsequent confirmation that all plume observations included targets inside the -3 dB beam width suggest that the physical presence and absence of plumes during survey passes are faithfully represented in the positioning and TS results.

Periods of consistent plume presence or absence were noted to change for several clusters between 2011 and 2012 (Figure 5). For example, a plume was observed at cluster 19 during all survey passes within the FOV in 2011 but only two passes (on both NNW and SSE headings) in 2012. The practical athwartship limit for plume detection at this cluster was not expected to be a factor in this observed change, as the two observations in 2012 were made on different headings and cluster 19 fell well within the FOV coverage estimate for all passes. Similarly, no plumes were observed at cluster 25 in 2011 but were frequently observed starting with pass 21 in 2012. These patterns suggest that gas flow at several clusters switches between “on” and “off” over time scales varying within and between each survey. Among consecutive plume observations at individual clusters with consistently detectable gas flow, the mean S_z values in the deepest 200 m appear to remain generally within ± 1 dB re 1 m^{-1} from pass to pass over time scales of 1 h to 7 months (e.g., Figure 5, cluster 4, passes 22–27; cluster 27, passes 12–18). Less frequently, larger S_z variations up to 10 dB re 1 m^{-1} were observed between subsequent passes separated by less than 2 h (e.g., Figure 5, cluster 11, passes 22–24). These observations suggest a high degree of variability in active gas flow at the seep study sites across all surveys.

At several locations along the survey lines there are groups of consecutively numbered clusters falling within a beam width footprint on the seafloor of each other, from which a maximum of one plume is observed per group per survey pass. These groups include clusters (4 and 5), (6 and 7), (8 and 9), (10 and 11), (21 through 24), (27 and 28), and (31 through 33). The general pattern of plume observations at only one cluster in each group per survey pass suggests possible connections of subseafloor gas migration pathways feeding the separately clustered seep sites in each group, by which gas tends to flow at only one of the clusters within each group at any given time. Likewise, instances of no plume observation during a pass over each group may be associated with gas flow at nearby gas vent sites outside the FOV coverage or a temporarily halt in gas flow while pressure builds sufficiently in a subseafloor gas pocket to restart acoustically observable bubble release; these scenarios cannot be explored further without additional water column and subbottom survey data.

5. Conclusions

A method for bubble plume detection and positioning has been demonstrated with a split-beam scientific echo sounder (SBES) employed for repeat surveys over a region of natural methane gas bubble venting at

approximately 1400 m depth in the northern Gulf of Mexico. Though gas flux cannot be established from TS measurements at a single frequency without knowledge of the bubble size distribution, a unit S_z equal to the TS normalized for the vertical extent of plume axis ensonification was employed to facilitate relative comparison of gas flux under the assumption of constant bubble size distribution. S_z also enables comparison of acoustic scattering strengths of plumes observed in other studies with different echo sounder configurations, such as transducer orientations and pulse lengths. In this study, plume behavior at known vent sites was observed to vary from apparently steady gas flow during surveys 8 months apart to multiple apparent starts and stops in gas flow on time scales of hours. Plumes were observed at an average of approximately one third of the known vent sites during each survey pass, indicating large spatial and temporal variability and suggesting that single-pass surveys do not adequately capture the nature of gas flow over large regions of the seafloor. Following the bubble plumes upward from the seafloor, only 20% of plumes were observed to reach depths of 600 m or shallower, where scattering from biological organisms in the deep scattering layer may have masked the acoustic returns from gas bubbles. The survival of bubbles detectable at 18 kHz during the 800 m ascent from 1400 to 600 m depth is followed by rapid extinction, suggesting inhibition of gas transfer during initial ascent by methane hydrate coatings on bubbles deeper than the shallow limit of the hydrate stability zone at approximately 600 m. With knowledge of bubble size distribution, S_z data incorporating reduced uncertainties of positioning and backscattering strength offer a step toward standardized gas flux calculation across seep investigations and echo sounder configurations.

Acknowledgments

Echo sounder data used in this paper were collected during NOAA Ship *Okeanos Explorer* cruises EX1105 (2011) and EX1202 Leg 3 (2012) and are publicly available by various methods. MBES and sound speed profile data are available through the NOAA OER Digital Atlas. A direct link is under development for access to SBES data through the NOAA OER Digital Atlas. At the time of submission, SBES data are available by request using the NOAA OER Program Data Access Request Form. This work was supported by the NOAA grants NA05NOS4001153 and NA10NOS4000073. We thank the captain, crew, and scientific personnel of NOAA Ship *Okeanos Explorer* for their efforts during data collection. Additionally, we thank Dezhong Chu for providing software to calculate calibration sphere target strength and Larry Mayer, Brian Calder, Jens Greinert, Helen Czerski, and one anonymous reviewer for their helpful comments on this manuscript.

References

- Artemov, Y. G. (2006), Software support for investigation of natural methane seeps by hydroacoustic method, *Mar. Ecol. J.*, *5*, 57–71.
- Artemov, Y. G., V. N. Egorov, G. G. Polikarpov, and S. B. Gulina (2007), Methane emission to the hydro- and atmosphere by gas bubble streams in the Dnieper paleo-delta, the Black Sea, *Mar. Ecol. J.*, *6*(3), 5–26.
- Chen, L., E. D. Sloan, C. A. Koh, and A. K. Sum (2014), Methane hydrate formation and dissociation on suspended gas bubbles in water, *J. Chem. Eng. Data*, *59*, 1045–1051.
- Clay, C. S., and H. Medwin (1977), *Acoustical Oceanography*, John Wiley, N. Y.
- Foote, K. G., H. P. Knudsen, and G. Vestnes (1987), *Calibration of Acoustic Instruments for Fish Density Estimation: A Practical Guide*, International Council for the Exploration of the Sea, Copenhagen.
- Francois, R. E., and G. R. Garrison (1982a), Sound absorption based on ocean measurements. Part I: Pure water and magnesium sulfate contributions, *J. Acoust. Soc. Am.*, *72*(3), 896–907.
- Francois, R. E., and G. R. Garrison (1982b), Sound absorption based on ocean measurements. Part II: Boric acid contribution and equation for total absorption of sound, *J. Acoust. Soc. Am.*, *72*(6), 1879–1890.
- Greinert, J. (2008), Monitoring temporal variability of bubble release at seeps: The hydroacoustic swath system GasQuant, *J. Geophys. Res.*, *113*, C07048, doi:10.1029/2007JC004704.
- Greinert, J., and B. Nützel (2004), Hydroacoustic experiments to establish a method for the determination of methane bubble fluxes at cold seeps, *Geo Mar. Lett.*, *24*(2), 75–85, doi:10.1007/s00367-003-0165-7.
- Greinert, J., Y. Artemov, V. Egorov, M. Debatist, and D. McGinnis (2006), 1300-m-high rising bubbles from mud volcanoes at 2080 m in the Black Sea: Hydroacoustic characteristics and temporal variability, *Earth Planet. Sci. Lett.*, *244*(1–2), 1–15, doi:10.1016/j.epsl.2006.02.011.
- Greinert, J., K. B. Lewis, J. Bialas, I. A. Pecher, A. Rowden, D. A. Bowden, M. De Batist, and P. Linke (2010), Methane seepage along the Hikurangi Margin, New Zealand: Overview of studies in 2006 and 2007 and new evidence from visual, bathymetric and hydroacoustic investigations, *Mar. Geol.*, *272*(1–4), 6–25, doi:10.1016/j.margeo.2010.01.017.
- Hickman, S. H., P. A. Hsieh, W. D. Mooney, C. B. Enomoto, P. H. Nelson, L. A. Mayer, T. C. Weber, K. Moran, P. B. Flemings, and M. K. McNutt (2012), Scientific basis for safely shutting in the Macondo Well after the April 20, 2010 Deepwater Horizon blowout, *Proc. Natl. Acad. Sci. U. S. A.*, *109*(50), 20,268–20,273, doi:10.1073/pnas.1115847109.
- Holland, C. W., T. C. Weber, and G. Etiope (2006), Acoustic scattering from mud volcanoes and carbonate mounds, *J. Acoust. Soc. Am.*, *120*(6), 3553–3565, doi:10.1121/1.2357707.
- Hornafius, J. S., D. Quigley, and B. P. Luyendyk (1999), The world's most spectacular marine hydrocarbon seeps (Coal Oil Point, Santa Barbara Channel, California): Quantification of emissions, *J. Geophys. Res.*, *104*(C9), 20,703–20,711.
- Hovland, M., S. Jensen, and C. Fichler (2012), Methane and minor oil macro-seep systems—Their complexity and environmental significance, *Mar. Geol.*, *332–334*, 163–173, doi:10.1016/j.margeo.2012.02.014.
- Johansen, Ø., H. Rye, and C. Cooper (2003), DeepSpill—Field study of a simulated oil and gas blowout in deep water, *Spill Sci. Technol. Bull.*, *8*(5–6), 433–443, doi:10.1016/S1353-2561(02)00123-8.
- Jones, A. T., J. Greinert, D. A. Bowden, I. Klauke, C. J. Petersen, G. L. Netzeband, and W. Weinrebe (2010), Acoustic and visual characterisation of methane-rich seabed seeps at Omakere Ridge on the Hikurangi Margin, New Zealand, *Mar. Geol.*, *272*(1–4), 154–169, doi:10.1016/j.margeo.2009.03.008.
- Judd, A. G. (2003), The global importance and context of methane escape from the seabed, *Geo Mar. Lett.*, *23*(3–4), 147–154, doi:10.1007/s00367-003-0136-z.
- Judd, A. G. (2004), Natural seabed gas seeps as sources of atmospheric methane, *Environ. Geol.*, *46*(8), 988–996, doi:10.1007/s00254-004-1083-3.
- Judd, A. G., M. Hovland, L. I. Dimitrov, S. G. Gil, and V. Jukes (2002), The geological methane budget at Continental Margins and its influence on climate change, *Geofluids*, *2*, 109–126.
- Kannberg, P. K., A. M. Tréhu, S. D. Pierce, C. K. Paull, and D. W. Cares (2013), Temporal variation of methane flares in the ocean above Hydrate Ridge, Oregon, *Earth Planet. Sci. Lett.*, *368*, 33–42, doi:10.1016/j.epsl.2013.02.030.
- Leifer, I., and I. MacDonald (2003), Dynamics of the gas flux from shallow gas hydrate deposits: Interaction between oily hydrate bubbles and the oceanic environment, *Earth Planet. Sci. Lett.*, *210*(3–4), 411–424, doi:10.1016/S0012-821X(03)00173-0.

- Leifer, I., J. R. Boles, B. P. Luyendyk, and J. F. Clark (2004), Transient discharges from marine hydrocarbon seeps: Spatial and temporal variability, *Environ. Geol.*, *46*(8), 1038–1052, doi:10.1007/s00254-004-1091-3.
- MacDonald, I. R., W. W. Sager, and M. B. Peccini (2003), Gas hydrate and chemosynthetic biota in mounded bathymetry at mid-slope hydrocarbon seeps: Northern Gulf of Mexico, *Mar. Geol.*, *198*(1–2), 133–158, doi:10.1016/S0025-3227(03)00098-7.
- McGinnis, D. F., J. Greinert, Y. Artemov, S. E. Beaubien, and A. Wüest (2006), Fate of rising methane bubbles in stratified waters: How much methane reaches the atmosphere?, *J. Geophys. Res.*, *111*, C09007, doi:10.1029/2005JC003183.
- Mienert, J. (2012), Signs of instability, *Nature*, *490*, 491–492.
- Milkov, A. V., R. Sassen, I. Novikova, and E. Mikhailov (2000), Gas hydrates at minimum stability water depths in the Gulf of Mexico: Significance to geohazard assessment, *Trans. Gulf Coast Assoc. Geol. Soc.*, *50*, 217–224.
- Naudts, L., J. Greinert, Y. Artemov, P. Staelens, J. Poort, P. Van Rensbergen, and M. De Batist (2006), Geological and morphological setting of 2778 methane seeps in the Dnepr paleo-delta, northwestern Black Sea, *Mar. Geol.*, *227*(3–4), 177–199, doi:10.1016/j.margeo.2005.10.005.
- Nikolovska, A., H. Sahling, and G. Bohrmann (2008), Hydroacoustic methodology for detection, localization, and quantification of gas bubbles rising from the seafloor at gas seeps from the eastern Black Sea, *Geochem. Geophys. Geosyst.*, *9*, Q10010, doi:10.1029/2008GC002118.
- Ostrovsky, I., D. F. McGinnis, L. Lapidus, and W. Eckert (2008), Quantifying gas ebullition with echosounder: The role of methane transport by bubbles in a medium-sized lake, *Limnol. Oceanogr. Methods*, *6*, 105–118, doi:10.4319/lom.2008.6.105.
- Rehder, G., P. W. Brewer, E. T. Peltzer, and G. Friederich (2002), Enhanced lifetime of methane bubble streams within the deep ocean, *Geophys. Res. Lett.*, *29*(15), 1731, doi:10.1029/2001GL013966.
- Römer, M., H. Sahling, T. Pape, G. Bohrmann, and V. Spieß (2012), Quantification of gas bubble emissions from submarine hydrocarbon seeps at the Makran continental margin (offshore Pakistan), *J. Geophys. Res.*, *117*, C10015, doi:10.1029/2011JC007424.
- Sahling, H., et al. (2009), Vodyanitskii mud volcano, Sorokin trough, Black Sea: Geological characterization and quantification of gas bubble streams, *Mar. Pet. Geol.*, *26*(9), 1799–1811, doi:10.1016/j.marpetgeo.2009.01.010.
- Sauter, E. J., S. I. Muyakshin, J. Charlou, and M. Schlüter (2006), Methane discharge from a deep-sea submarine mud volcano into the upper water column by gas hydrate-coated methane bubbles, *Earth Planet. Sci. Lett.*, *243*, 354–365.
- Schneider von Deimling, J., G. Rehder, J. Greinert, D. F. McGinnis, A. Boetius, and P. Linke (2011), Quantification of seep-related methane gas emissions at Tommeliten, North Sea, *Cont. Shelf Res.*, *31*(7–8), 867–878, doi:10.1016/j.csr.2011.02.012.
- Tishchenko, P., C. Hensen, K. Wallmann, and C. S. Wong (2005), Calculation of the stability and solubility of methane hydrate in seawater, *Chem. Geol.*, *219*(1–4), 37–52, doi:10.1016/j.chemgeo.2005.02.008.
- Towler, R. (2010), readEKRaw EK/ES60 ME/MS70 MATLAB toolkit, rel. 4/16/10. [Available at <http://hydroacoustics.net/viewtopic.php?f=36&t=131>.]
- Urick, R. J. (1975), *Principles of Underwater Sound*, 2nd ed., McGraw-Hill, N. Y.
- Weber, T. C., K. Jerram, and L. Mayer (2012a), Acoustic sensing of gas seeps in the deep ocean with split-beam echosounders, in *Proceedings of Meetings on Acoustics*, *17*(1), Acoustical Society of America. [Available at <http://scitation.aip.org/content/asa/journal/poma/17/1/10.1121/1.4772948>.]
- Weber, T. C., A. De Robertis, S. F. Greenaway, S. Smith, L. Mayer, and G. Rice (2012b), Estimating oil concentration and flow rate with calibrated vessel-mounted acoustic echo sounders, *Proc. Natl. Acad. Sci. U. S. A.*, *109*(50), 20,240–20,245, doi:10.1073/pnas.1108771108.
- Weber, T. C., L. Mayer, J. Beaudoin, K. Jerram, M. Malik, B. Shedd, and G. Rice (2012c), Mapping gas seeps with the deepwater multibeam echosounder on Okeanos Explorer, *Oceanography*, *25*(1), suppl., 54–55.
- Weber, T. C., L. Mayer, K. Jerram, J. Beaudoin, and Y. Rzhonov (2014), Acoustic estimates of methane gas flux from the seabed in a 6000 km² region in the Northern Gulf of Mexico, *Geochem. Geophys. Geosyst.*, *15*, 1911–1925, doi:10.1002/2014GC005271.